RSC Advances

PAPER

View Article Online
View Journal | View Issue

Check for updates

Cite this: *RSC Adv.*, 2021, **11**, 33149

MoS_2-assisted Fe^{2+}/peroxymonosulfate oxidation for the abatement of phenacetin: efficiency, mechanisms and toxicity evaluation†

Yu-qiong Gao, *[a] Yan-yan Rao,[a] Han Ning,[a] Da-qiang Yin[b] and Nai-yun Gao[b]

Received 3rd August 2021
Accepted 4th October 2021

DOI: 10.1039/d1ra05892d

rsc.li/rsc-advances

In this study, molybdenum disulfide (MoS_2) was chosen as a co-catalyst to enhance the removal efficiency of phenacetin (PNT) in water by a ferrous ion-activated peroxymonosulfate (Fe^{2+}/PMS) process. Operating parameters, such as the initial solution pH and chemical dose on PNT degradation efficiency were investigated and optimized. Under an initial pH of 3, an Fe^{2+} dose of 25 μM, a PMS dose of 125 μM and a MoS_2 dose of 0.1 g L^{-1}, the degradation efficiency of PNT reached 94.3%, within 15 min. The presence of common water constituents including Cl^-, HCO_3^-, SO_4^{2-} and natural organic matter (NOM) will inhibit degradation of PNT in the MoS_2/Fe^{2+}/PMS system. Radical quenching tests combined with electron paramagnetic resonance (EPR) results indicated that in addition to free radical species ($^{\bullet}OH$, $SO_4^{\bullet-}$ and $O_2^{\bullet-}$), nonradical reactive species ($^1O_2$) were also crucial for PNT degradation. The variations in the composition and crystalline structure of the MoS_2 before and after the reaction were characterized by XPS and XRD. Further, the degradation pathways of PNT were proposed according to the combined results of LC/TOF/MS and DFT calculations, and primarily included hydroxylation of the aromatic ring, cleavage of the C–N bond of the acetyl-amino group, and cleavage of the C–O bond of the ethoxy group. Finally, toxicity assessment of PNT and its products was predicted using the ECOSAR program.

Open Access Article. Published on 08 October 2021. Downloaded on 12/29/2025 11:10:09 AM.
This article is licensed under a Creative Commons Attribution-NonCommercial 3.0 Unported Licence.

1. Introduction

The use of pharmaceutical and personal care products (PPCPs), such as antibiotics, care products, and medical drugs, has increased gradually in recent decades. However, because the traditional water treatment process cannot effectively remove these organic contaminants, the residues of PPCPs have been frequently detected in natural water and may pose a potential threat to our ecosystem and human health.[1] The sources of PPCPs in natural water mainly include hospitals, pharmaceutical industries, domestic wastewater, agricultural activities, *etc.*2 As a typical PPCP with anti-inflammatory and analgesic effects, phenacetin (PNT), also known as *N*-(4-ethoxyphenyl) acetamide, has been widely detected in natural water. Due to its high solubility, multiple pK_a values and resistance to microbial degradation in traditional wastewater treatment, PNT was detected at μg L^{-1} concentrations in wastewater treatment plants (WWTPs) and even in surface waters with concentrations at the ng L^{-1} level.[3,4] Previous studies indicated that long-term exposure to PNT may result in side effects in aquatic organisms and on human health, such as anemia, cyanosis, hypoxia, kidney damage, and even cancer.[5] Thus, it is essential to develop a reasonable and effective way to remove PNT from water.

Currently, advanced oxidation processes, abbreviated AOPs, have attracted increasing attention due to their successful application to decompose PPCPs in water by generating highly reactive radical species, *i.e.*, hydroxyl radical ($^{\bullet}OH$).[6] More recently, sulfate radical ($SO_4^{\bullet-}$)-based AOPs have gained popularity for the treatment of PPCPs in water owing to their comparable standard redox potential (E_0 = 2.5–3.1 V) with that of $^{\bullet}OH$ (E^0 = 2.8 V).[7,8] In addition, $SO_4^{\bullet-}$ was more selective than $^{\bullet}OH$, making $SO_4^{\bullet-}$-based AOPs less impacted by the presence of common inorganic anions and natural organic matter (NOM).[9] Persulfate (PS) and peroxymonosulfate (PMS) are the two common sources for generating $SO_4^{\bullet-}$. PS and PMS, which have redox potentials of 2.01 V and 1.82 V, respectively, are powerful oxidizers.[10] Nonetheless, PS or PMS cannot directly oxidize organic contaminants efficiently owing to their low reaction rates with target compounds at ambient temperatures; therefore, proper activation methods, such as thermal activation, UV irradiation, and transition metal activation, are needed for PS and PMS.[10]

[a]*School of Environment and Architecture, University of Shanghai for Science and Technology, Shanghai 200093, China*

[b]*State Key Laboratory of Pollution Control and Resource Reuse, College of Environmental Science and Engineering, Tongji University, Shanghai 200092, China. E-mail: gaoyq@usst.edu.cn; Tel: +86 21 55275979*

† Electronic supplementary information (ESI) available. See DOI: 10.1039/d1ra05892d

© 2021 The Author(s). Published by the Royal Society of Chemistry

Open Access Article. Published on 08 October 2021. Downloaded on 12/29/2025 11:10:09 AM. This article is licensed under a Creative Commons Attribution-NonCommercial 3.0 Unported Licence.

Ferrous ion (Fe^{2+})-activated peroxymonosulfate (Fe^{2+}/PMS) is one of the most regularly used $SO_4^{\cdot-}$-based AOPs attributable to its simple operation, low cost, and nontoxicity. In the Fe^{2+}/PMS oxidation process, the degradation of organic contaminants always takes place in two stages: a fast stage during the initial period of the reaction and then a slow stage during the following reaction. During the initial stage, Fe^{2+} is oxidized to Fe^{3+} extremely readily, whereas the poor recovery of Fe^{2+} during the reaction leads to the lack of Fe^{2+} available for PMS activation.[11] Thus, the usage efficiency of Fe^{2+} in the Fe^{2+}/PMS system is not sufficient.[12] To facilitate the transformation of Fe^{3+} to Fe^{2+}, many methods have been extensively studied in recent years. For example, to maintain a proper amount of Fe^{2+} in the Fe^{2+}/PMS system, zero-valent iron (ZVI) was always selected as an alternative to Fe^{2+} because it could generate Fe^{2+} more slowly by corrosion and then reduce Fe^{3+} to Fe^{2+} on the ZVI surface.[13] In addition, chelating agents such as ethylenediamine tetraacetic acid (EDTA),[14] ethylenediamine-*N*,*N*′-disuccinic acid (EDDS),[15] and nitrilotriacetic acid (NTA)[16,17] can complex with Fe^{2+} and slow its release, thus slowly catalyzing the reaction and improving the usage efficiency of Fe^{2+}. Recently, as a vital member of transition metal dichalcogenides, MoS_2 has received great attention because of its excellent performance in environmental remediation.[18] Notably, MoS_2 has been proven to promote the conversion of Fe^{3+} to Fe^{2+} and directly activate PMS to produce a certain amount of $SO_4^{\cdot-}$, enhancing the degradation efficiency of contaminants.[19] Simultaneously, previous studies have also proved that MoS_2, as a co-catalyst, can be recycled and reused.[20–22] Therefore, the MoS_2-assisted Fe^{2+}/PMS oxidation process is a promising method to apply to PPCP-polluted water.

The purpose of this study was to investigate the performance and mechanism of the degradation of PNT by the MoS_2/Fe^{2+}/PMS system. Various parameters, such as Fe^{2+} dose, MoS_2 dose and PMS dose, were investigated to optimize the process. The effects of initial solution pH, common anions (Cl^- and HCO_3^-), and NOM on the PNT degradation performance were also evaluated. The reactive radical species responsible for PNT degradation were identified and analyzed. The chemical state of MoS_2 before and after the reaction was measured by using XRD and XPS. Further, the degradation pathways of PNT were proposed based on LC/TOF/MS technique and density functional theory (DFT) calculation. Finally, the toxicity of PNT and its degradation products were assessed by Ecological Structure–Activity Relationships (ECOSAR) program.

2. Materials and methods

2.1. Chemicals and reagents

Phenacetin (PNT, ≥98.0%), *p*-benzoquinone (*p*-BQ, ≥98.0%) and humic acid (HA) were purchased from Sigma-Aldrich (USA). Molybdenum sulfide (MoS_2, 99.5%, <2 μm), PMS ($KHSO_5 \cdot 0.5KHSO_4 \cdot 0.5K_2SO_4$), 5,5-dimethyl-1-pyrroline (DMPO, >99.0%) and 2,2,6,6-tetramethylpiperidine were purchased from Aladdin Chemistry Co., Ltd. (Shanghai, China). $FeSO_4 \cdot 7H_2O$ (≥99.0%), sulfuric acid (H_2SO_4, ≥95.0%), sodium hydroxide (NaOH, ≥96.0%), sodium chloride (NaCl, ≥99.5%), sodium bicarbonate ($NaHCO_3$, ≥99.5%), *tert*-butanol (TBA, ≥98.0%), and ethanol (EtOH, ≥99.5%) were provided by Sinopharm Chemical Reagent Co., Ltd. (Shang, China). All solutions were freshly prepared using Milli-Q purified water.

2.2. Experimental procedures

Batch experiments were conducted in an amber wide-mouth bottle containing 250 mL of reaction solution with magnetic stirring at 300 rpm at room temperature (20 ± 1 °C). In a typical run, a certain amount of MoS_2 was added to the mixed solution of PNT and $FeSO_4$, followed by 30 s of ultrasonic treatment to form a dispersion, which increased the contact area between the MoS_2 and the reaction solution. The reaction was initiated by adding a certain amount of PMS into the solution. The initial solution pH was adjusted by adding 0.1 M H_2SO_4 or NaOH. At different time intervals, 1 mL samples were taken and immediately mixed with ethanol to terminate the reaction, and then the sample was filtered through a 0.22 μm membrane before further analysis. All the tests were performed at least in triplicate, and the results were averaged.

2.3. Analytical method

The concentration of PNT was measured by using HPLC (Waters e2695, USA) equipped with a UV detector set at 240 nm and a C18 column (250 mm × 4.6 mm, 5 μm, Agela Technologies) maintained at 35 °C. The mobile phase consisted of acetonitrile and water (40 : 60, v/v) at a flow rate of 0.8 mL min^{-1}, and the injection volume was 20 μL.

Electron paramagnetic resonance (EPR) measurements were obtained on an EPR spectrometer (Bruker A300, Germany). X-ray photoelectron spectroscopy (XPS) was performed on a Thermo Scientific K-Alpha, and X-ray powder diffraction (XRD) patterns were determined using an X-ray diffractometer (Rigaku Ultima IV).

The PNT degradation products were identified using LC/TOF/MS (Agilent 1290 UPLC/6550 Q-TOF) in positive ionization mode using an electrospray ionization (ESI) source. Separation was accomplished using a Waters BEH C18 column (2.1 × 100 mm, 1.7 μm) with gradient elution, and the flow rate was set at 0.3 mL min^{-1}. The mobile phase consisted of ultrapure water (A) and acetonitrile (B), and the gradient mode was programmed as follows: (1) 90% of A was maintained in the first 1 min; (2) from 1 to 9 min, A was linearly decreased from 90% to 10%, then kept for 3 min; (3) from 12 to 12.1 min, A and B were returned to the initial status, and then maintained for 0.9 min. The spray voltage, sheath gas temperature, and sheath gas flow were set at 4000 V, 350 °C, and 12 L min^{-1}, respectively.

2.4. DFT calculation and toxicity assessment

Density functional theory (DFT) calculations (Gaussian 09) were used to predict the degradation products and transformation pathways of PNT using the B3LYP/6-311G basis set. The acute and chronic toxicity of PNT and its degradation products to fish, daphnia, and green algae were predicted by using ECOSAR program.

© 2021 The Author(s). Published by the Royal Society of Chemistry

Open Access Article. Published on 08 October 2021. Downloaded on 12/29/2025 11:10:09 AM.
This article is licensed under a Creative Commons Attribution-NonCommercial 3.0 Unported Licence.

3. Results and discussion

3.1. Acceleration of PNT degradation by Fe^{2+}/PMS by MoS_2

Fig. 1 compares the degradation of PNT in different systems, *i.e.*, PMS alone, Fe^{2+} alone, MoS_2 alone, MoS_2/Fe^{2+}, MoS_2/PMS, Fe^{2+}/PMS, and MoS_2/Fe^{2+}/PMS processes. After 15 min, the degradation of PNT by PMS or Fe^{2+} alone was negligible. The application of MoS_2 and MoS_2/Fe^{2+} also resulted in PNT removal within 5%, which indicated that PNT is resistant to the absorption of MoS_2. Furthermore, the MoS_2/PMS and Fe^{2+}/PMS systems achieved PNT removal of 32.9% and 23.1%, respectively, showing that both Fe^{2+} and MoS_2 could effectively activate PMS to produce $SO_4^{\cdot-}$ and/or $^{\cdot}OH$, which account for PNT degradation (eqn (1)–(3)).[12,19] During the Fe^{2+}/PMS process, the PNT degradation slows suddenly after a period of reaction due to the fast consumption of Fe^{2+} and poor reduction of Fe^{3+} to Fe^{2+}.[11] Notably, the obvious enhancement of PNT degradation was observed by adding MoS_2 to the Fe^{2+}/PMS system, which resulted in a removal rate of 94.3% within 15 min, demonstrating the promoting effect of MoS_2 in the Fe^{2+}/PMS system. Additional experiments were also performed to estimate the role of MoS_2 in the Fe^{3+}/PMS system (Fig. S1†), and it was found that approximately 72.0% removal of PNT was also achieved in the MoS_2/Fe^{3+}/PMS system, which demonstrated the transformation of Fe^{3+} to Fe^{2+} in the presence of MoS_2 (eqn (4)) since Fe^{3+} cannot serve as an efficient activator of PMS. A similar phenomenon was also reported for 2,4,6-trichlorophenol (TCP) and sulfamethoxazole (SMX) degradation in the Fe^{2+}/PMS system by adding MoS_2.[20,22] It is generally believed that the unsaturated S atoms on the MoS_2 surface can capture protons to form H_2S and meanwhile expose Mo^{4+}, which could accelerate the Fe^{3+}/Fe^{2+} conversion (eqn (4)) and facilitate PMS conversion (eqn (3)), thus significantly improving the decomposition of PMS.[23]

$$Fe^{2+} + HSO_5^- \rightarrow SO_4^{\cdot-} + Fe^{3+} + OH^- \quad (1)$$

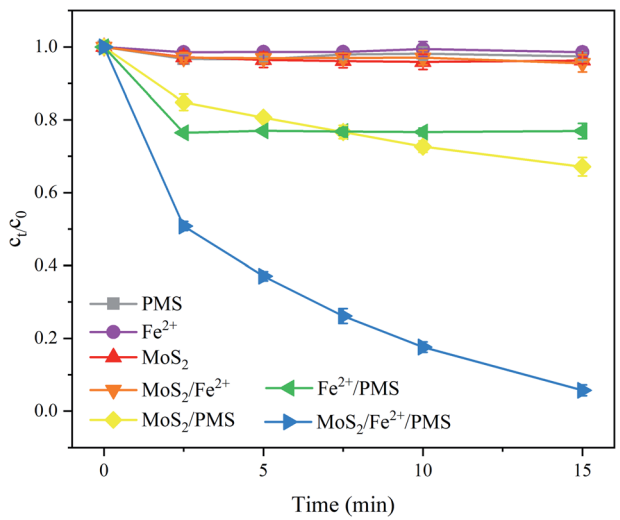

Fig. 1 Degradation of PNT in different systems. Experimental conditions: $[PNT]_0 = 25\ \mu M$, $pH_0 = 3.0$, $[Fe^{2+}]_0 = 25\ \mu M$, $[PMS]_0 = 125\ \mu M$, $[MoS_2]_0 = 0.1\ g\ L^{-1}$.

$$Fe^{2+} + HSO_5^- \rightarrow {\cdot}OH + Fe^{3+} + SO_4^{2-} \quad (2)$$

$$\text{Interface: } Mo^{4+} + HSO_5^- \rightarrow SO_4^{\cdot-} + Mo^{6+} + OH^- \quad (3)$$

$$\text{Interface: } Mo^{4+} + 2Fe^{3+} \rightarrow Mo^{6+} + 2Fe^{2+} \quad (4)$$

3.2. Optimal conditions

The solution pH has a complex role in the degradation of organic contaminants in $SO_4^{\cdot-}$-based AOPs, as it may affect the formation of reactive oxidizing species and the stability of PMS.[24] Thus, it is necessary to evaluate the effect of the initial solution pH on the PNT degradation performance of the MoS_2/Fe^{2+}/PMS system. The effect of the initial solution pH on PNT degradation is illustrated in Fig. 2(a). As clearly seen, acidic conditions are more beneficial to PNT degradation than neutral or alkaline conditions. However, the inhibition of PNT degradation was observed at an extremely acidic pH (pH = 2). When the initial solution pH was decreased to 2, the generated radicals, such as $SO_4^{\cdot-}$ and $^{\cdot}OH$, were consumed by excess hydrogen ions according to eqn (5) and (6).[25] Furthermore, the formation of $(Fe(H_2O))2^+$ at an acidic pH negatively influenced PNT degradation because the free Fe^{2+} was reduced.[26] As the initial solution pH increased from 3 to 9, the Fe^{3+} in the reaction system converted to the insoluble ferric hydroxide, which arrested the reduction of Fe^{3+} to Fe^{2+}, thereby affecting PMS activation. Moreover, PMS dissociation increased through nonradical pathways at higher solution pH.[27] In addition, under basic conditions, edge S would not dissociate, and as a result, S could not be captured, thus hindering the exposure of the Mo(IV) atom. Finally, MoS_2 was negatively charged when the pH was higher, leading to strong repulsion between MoS_2 and PMS, which could also hinder the PNT degradation.[28]

$$SO_4^{\cdot-} + H^+ + e^- \rightarrow HSO_4^{\cdot-} \quad (5)$$

$$^{\cdot}OH + H^+ + e^- \rightarrow H_2O \quad (6)$$

The effect of the Fe^{2+} dose on PNT degradation is shown in Fig. 2(b). As shown, the removal rate of PNT increased markedly from 32.9% to 94.3% with increasing Fe^{2+} dose from 0 to 25 μM. As the Fe^{2+} dose further increased to 50 μM, the removal rate of PNT slightly increased to 95.4%. However, when the Fe^{2+} dose reached 100 μM, the removal rate of PNT decreased to 75.0%. Briefly, the removal rate of PNT gradually increased when the molar ratio of $[Fe^{2+}]_0/[MoS_2]_0 \leq 1:25$, while further increased the molar ratio of $[Fe^{2+}]_0/[MoS_2]_0$ did not exhibited an obvious beneficial for PNT degradation or even decreased the removal rate of PNT. It is generally acknowledged that a large amount of Fe^{2+} corresponds to more PMS activator availability, which results in a faster reaction rate. However, excess Fe^{2+} also consumes reactive radicals (eqn (7) and (8)), slowing down the PNT degradation.[29] Therefore, based on the activation efficiency along with the chemical cost, the optimum dose of Fe^{2+} was set to 25 μM ($[Fe^{2+}]_0/[MoS_2]_0 = 1:25$) in this study.

© 2021 The Author(s). Published by the Royal Society of Chemistry

Open Access Article. Published on 08 October 2021. Downloaded on 12/29/2025 11:10:09 AM.
This article is licensed under a Creative Commons Attribution-NonCommercial 3.0 Unported Licence.

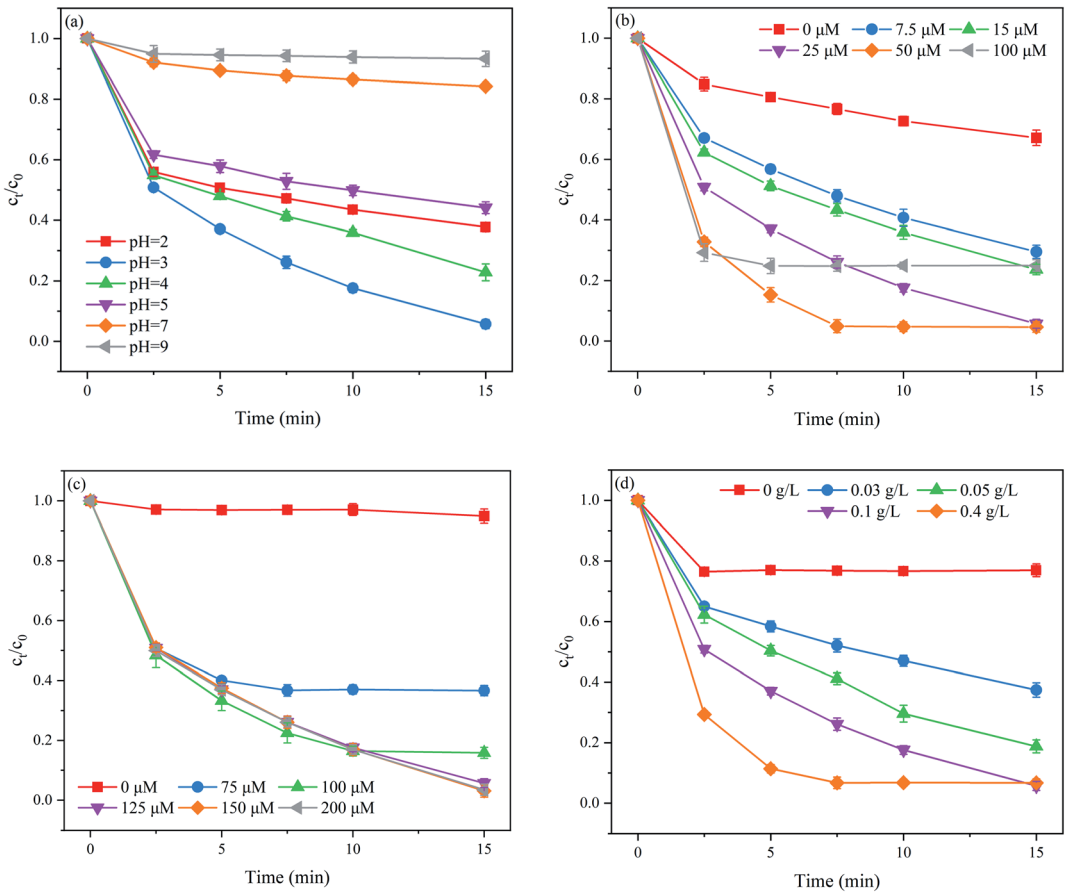

Fig. 2 Effects of (a) the initial solution pH, (b) Fe^{2+} dose, (c) PMS dose, and (d) MoS_2 dose on PNT degradation in the MoS_2/Fe^{2+}/PMS process. Experimental conditions: $[PNT]_0 = 25$ μM; (a) $[Fe^{2+}]_0 = 25$ μM, $[PMS]_0 = 125$ μM, $[MoS_2]_0 = 0.1$ g L; (b) $pH_0 = 3.0$, $[PMS]_0 = 125$ μM, $[MoS_2]_0 = 0.1$ g L; (c) $pH_0 = 3.0$, $[Fe^{2+}]_0 = 25$ μM, $[MoS_2]_0 = 0.1$ g L; (d) $pH_0 = 3.0$, $[Fe^{2+}]_0 = 25$ μM, $[PMS]_0 = 125$ μM.

$$Fe^{2+} + SO_4^{\cdot -} \rightarrow Fe^{3+} + SO_4^{2-} \quad (7)$$

$$Fe^{2+} + {}^{\cdot}OH \rightarrow Fe^{3+} + H_2O \quad (8)$$

The PMS dose plays a vital role in removing organic contaminants in $SO_4^{\cdot -}$-based AOPs, as it serves as the primary source of reactive radicals. The effect of the PMS dose on PNT degradation is shown in Fig. 2(c). As shown, the removal rate of PNT increased from 5.1% to 94.3% as the PMS dose increased from 0 to 125 μM. However, the continuous increase in PMS dose did not further improve the removal rate of PNT. This phenomenon may be ascribed to the quenching effect of $SO_4^{\cdot -}$ by excess PMS and the self-recombination of $SO_4^{\cdot -}$ (eqn (9) and (10)).[27] Similar findings have been reported for the removal of SMX at different PMS doses in the MoS_2/Fe^{2+}/PMS system.[22]

$$HSO_5^- + SO_4^{\cdot -} \rightarrow SO_5^{\cdot -} + SO_4^{2-} + H^+ \quad (9)$$

$$SO_4^{\cdot -} + SO_4^{\cdot -} \rightarrow S_2O_8^{2-} \quad (10)$$

The effect of the MoS_2 dose on PNT degradation is shown in Fig. 2(d). As shown, the removal rate of PNT increased monotonically from 23.1% to 94.3% as the MoS_2 content increased from 0 to 0.1 g L^{-1}. The number of exposed edge S atoms increased as the MoS_2 dose increased, and then more active sites were available to accelerate the Fe^{3+}/Fe^{2+} cycle, which facilitated the PNT degradation. Nevertheless, the removal rate of PNT slightly decreased when the MoS_2 was increased to 0.4 g L^{-1} because $Mo4^+$ acts as a scavenger of $SO_4^{\cdot -}$.[21]

3.3. Effects of common anions and NOM

Common anions (*e.g.*, Cl^-, HCO_3^-, and SO_4^{2-}) and natural organic matter (NOM) are universal in natural water bodies and have been demonstrated to influence target organic contaminant degradation during $SO_4^{\cdot -}$-based AOPs. Therefore, it is necessary to evaluate the impact of these water components on the degradation performance of PNT once applying the MoS_2/Fe^{2+}/PMS process to the treatment of PNT in natural waters. The effects of different concentrations of Cl^-, HCO_3^-, and HA on PNT degradation are shown in Fig. 3.

As shown in Fig. 3(a), Cl^- exerted an adverse effect on PNT degradation. The removal rate of PNT decreased from 93.0% to 78.6% as the concentration of Cl^- increased from 0 to 10 mM. In the presence of Cl^-, $SO_4^{\cdot -}$ was rapidly scavenged at high reaction rate constants to form reactive chlorine species (eqn. (11) and (12)) such as $Cl^{\cdot}$ and $Cl_2^{\cdot -}$, which exhibited lower redox potentials than $SO_4^{\cdot -}$.[30] As seen in Fig. 3(b), HCO_3^- also

© 2021 The Author(s). Published by the Royal Society of Chemistry

Open Access Article. Published on 08 October 2021. Downloaded on 12/29/2025 11:10:09 AM.
This article is licensed under a Creative Commons Attribution-NonCommercial 3.0 Unported Licence.

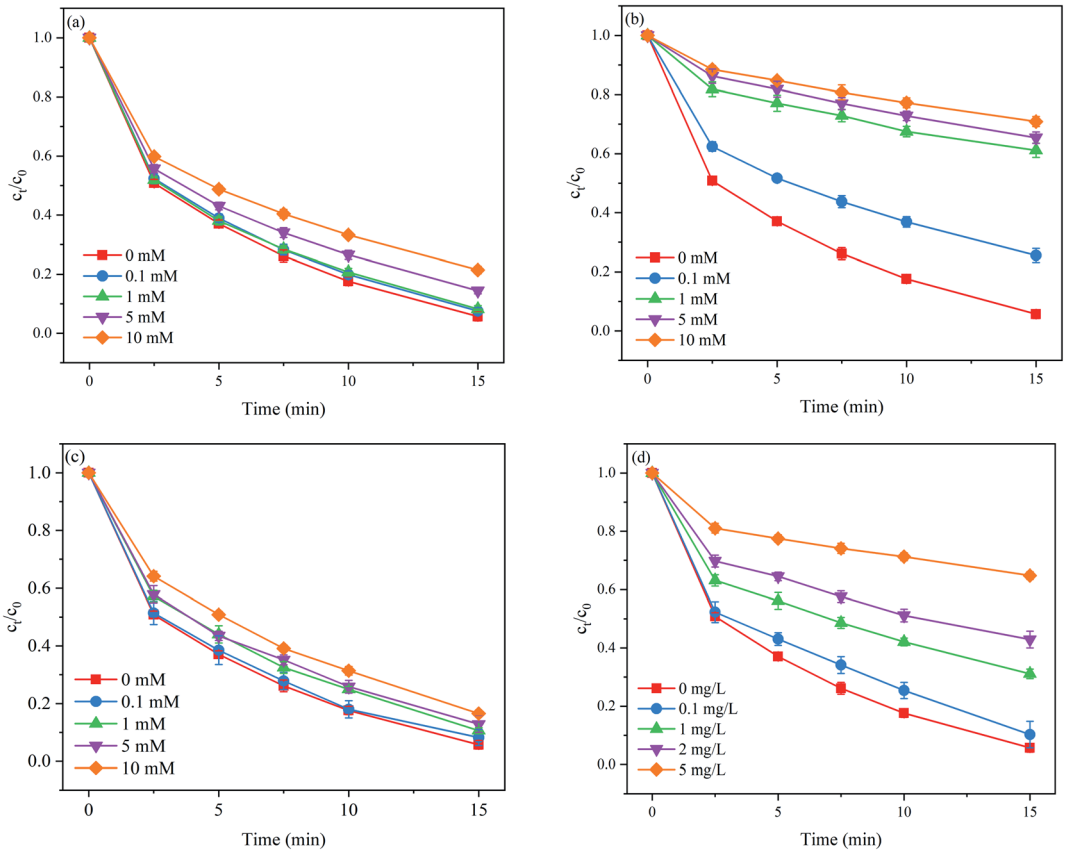

Fig. 3 Effects of (a) Cl^-, (b) HCO_3^-, (c) SO_4^{2-}, and (d) HA on PNT degradation in the MoS_2/Fe^{2+}/PMS process. Experimental conditions: $[PNT]_0$ = 25 μM, pH_0 = 3.0, $[Fe^{2+}]_0$ = 25 μM, $[PMS]_0$ = 125 μM, $[MoS_2]_0$ = 0.1 g L^{-1}.

exhibited adverse effects on PNT degradation. The removal rate of PNT decreased from 93.0% to 29.1% as the concentration of HCO_3^- increased from 0 to 10 mM. HCO_3^- is a well-known radical scavenger that can quench $SO_4^{\bullet-}$ and $^{\bullet}OH$ to produce less reactive radical species such as the carbonate radical ($CO_3^{\bullet-}$) (eqn. (13) and (14)).[31] HCO_3^- can also directly consume PMS *via* eqn (15).[32] In addition, the presence of HCO_3^- increased the solution pH, which was unfavorable to edge S atom capture. As seen in Fig. 3(c), the presence of SO_4^{2-} also inhibited the PNT degradation. The removal rate of PNT decreased from 93.0% to 83.5% as the concentration of SO_4^{2-} increased from 0 to 10 mM. The reason for this phenomenon lies in that the redox potential of $SO_4^{\bullet-}/SO_4^{2-}$ would decrease due to the presence of SO_4^{2-}.[33] As shown in Fig. 3(d), the removal rate of PNT decreased consistently from 93.0% to 35.2% as the concentration of HA increased from 0 to 5 mg L^{-1}. NOM hinders the performance of MoS_2/Fe^{2+}/PMS by scavenging $SO_4^{\bullet-}$ and $^{\bullet}OH$ because the electron-rich moieties of NOM readily react with these electrophilic radicals, resulting in a decrease in the free radicals available for PNT degradation.[34] These findings revealed that the impact of water characteristics should not be ignored once applying the MoS_2/Fe^{2+}/PMS process for practical use, and the operation parameters need to be carefully optimized to overcome the side effects caused by these water components in natural water.

$$Cl^- + SO_4^{\bullet-} \rightarrow Cl^{\bullet} + SO_4^{2-} \quad (11)$$

$$Cl^{\bullet} + Cl^- \rightarrow Cl_2^{\bullet-} \quad (12)$$

$$HCO_3^- + SO_4^{\bullet-} \rightarrow SO_4^{2-} + H^+ + CO_3^{\bullet-} \quad (13)$$

$$HCO_3^{\bullet-} + \cdot OH \rightarrow CO_3^{\bullet-} + H_2O \quad (14)$$

$$HCO_3^- + HSO_5^- \rightarrow HSO_4^{2-} + HCO_4^- \quad (15)$$

3.4. Identification of radical species

To investigate the role of radical species on PNT degradation, different quenchers, *i.e.* TBA, EtOH, *p*-BQ and TEMP were added to the MoS_2/Fe^{2+}/PMS system. TBA was selected as a $^{\bullet}OH$ scavenger because its reaction with $^{\bullet}OH$ had a rate constant that was approximately one thousand times faster ($(3.8–7.6) \times 10^8$ M^{-1} s^{-1}) than that of its reaction with $SO_4^{\bullet-}$ ($(4.0–9.1) \times 10^5$ M^{-1} s^{-1}).[35] As shown in Fig. 4(a), TBA slightly decreased the PNT removal rate. At 15 min, 67.5% was degraded with 50 mM TBA, which represents an efficiency that was 26.8% lower than that of the system without TBA. EtOH can significantly scavenge $^{\bullet}OH$ and $SO_4^{\bullet-}$ with second-order rate constants of $(1.2–2.8) \times 10^9$ and $(1.6–7.7) \times 10^7$ M^{-1} s^{-1}, respectively. After adding 50 mM EtOH, the PNT removal rate markedly decreased to 17.6%, which was 76.7% lower than that of PNT without a scavenger. *p*-BQ was added to the reaction solution to further investigate the role of $O_2^{\bullet-}$ because it can react with $O_2^{\bullet-}$

© 2021 The Author(s). Published by the Royal Society of Chemistry

Open Access Article. Published on 08 October 2021. Downloaded on 12/29/2025 11:10:09 AM.
This article is licensed under a Creative Commons Attribution-NonCommercial 3.0 Unported Licence.

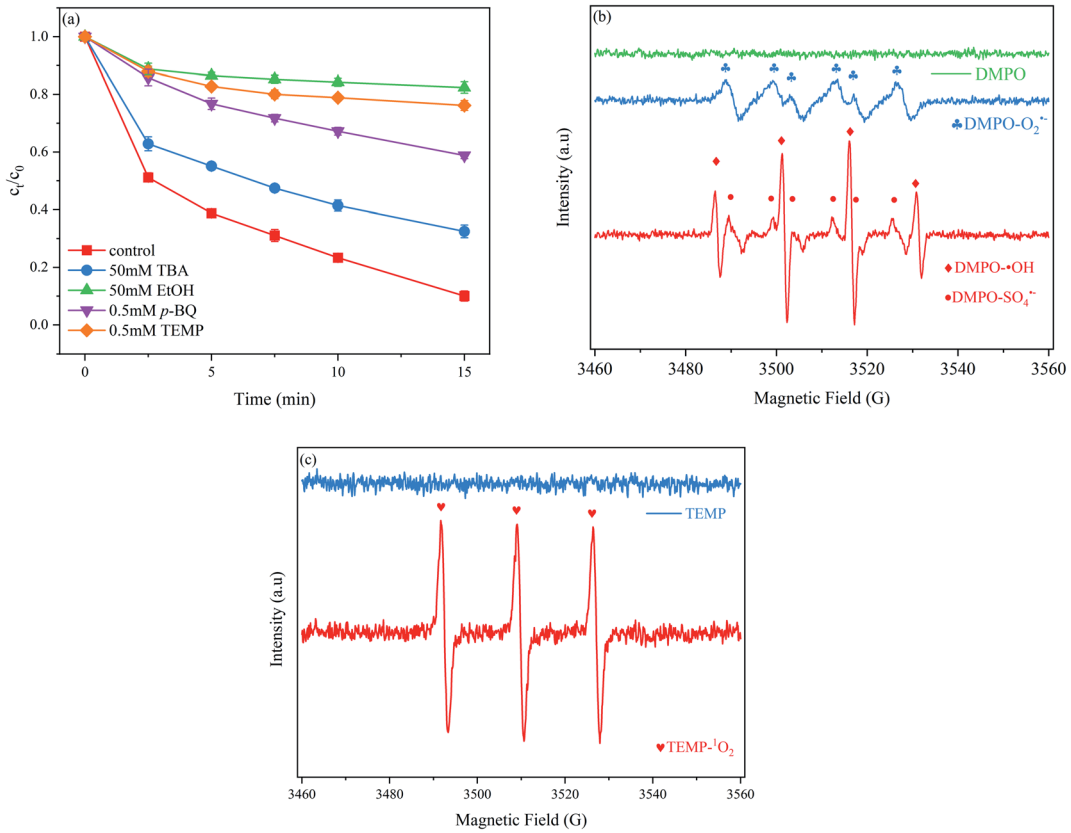

Fig. 4 (a) Effects of scavenger on PNT degradation; (b) EPR spectra of $O_2^{\bullet-}$ $^{\bullet}OH$ and $SO_4^{\bullet-}$ using DMPO and (c) EPR spectra of $^1O_2$ using TEMP. Experimental conditions: $[PNT]_0 = 25$ μM, $pH_0 = 3.0$, $[Fe^{2+}]_0 = 25$ μM, $[PMS]_0 = 125$ μM, $[MoS_2]_0 = 0.1$ g L^{-1}.

with a second-order rate constant of $(0.9–1.0) \times 10^9$ M^{-1} s^{-1}.[36] Our results show that the PNT removal rate decreased to 41.2% after the addition of 0.5 mM *p*-BQ, which indicated that $O_2^{\bullet-}$ also participated in the degradation of PNT. Next, TEMP was added to the reaction solution to investigate the behavior of $^1O_2$.[37] The results show that PNT degradation was obviously hindered in the presence of 0.5 mM TEMP. These results indicated that in addition to the commonly-reported $^{\bullet}OH$ and $SO_4^{\bullet-}$, a considerable amount of $^1O_2$ and $O_2^{\bullet-}$ is present in the MoS_2/Fe^{2+}/PMS system and simultaneously participates in the removal of PNT.

EPR was employed to directly detect the reactive species by using DMPO and TEMP as spin trap agents. DMPO could capture $^{\bullet}OH$, $SO_4^{\bullet-}$, and $O_2^{\bullet-}$ to form different spin adducts with respective signals,[38] while TEMP could capture $^1O_2$.[39] As shown in Fig. 4(b), no signal was detected in DMPO alone. In the MoS_2/Fe^{2+}/PMS system, four peaks with a 1 : 2 : 2 : 1 intensity ratio corresponding to the characteristic peak of DMPO–$^{\bullet}OH$ ($\alpha_H = \alpha_N = 14.9$ G) was observed, and six peaks with equal intensity corresponding to the characteristic peak of DMPO–$SO_4^{\bullet-}$ ($\alpha_N = 13.2$ G, $\alpha_H = 9.6$ G, $\alpha_H = 1.48$ G, $\alpha_N = 0.78$ G) was also observed. The relatively weak signal of DMPO–$SO_4^{\bullet-}$ was attributed to the lower sensitivity and shorter lifetime of the DMPO–$SO_4^{\bullet-}$ peak.[36] The peak of DMPO–$O_2^{\bullet-}$ ($\alpha_N = 17.4$ G) adduct was also clearly detected. Fig. 4(c) exhibits strong triplet peaks with equal intensities; these signals are attributed to TEMP–$^1O_2$ and demonstrate the generation of $^1O_2$ in the MoS_2/Fe^{2+}/PMS system. The EPR results were consistent with the results of the quenching experiments.

3.5. Characterization of MoS_2 before and after reaction

The XRD patterns of MoS_2 before and after reaction are given in Fig. S2.† The observed diffraction peaks were nearly unchanged after the reaction, and the peak positions were consistent with those reported by Xing *et al.*,[18] reflecting the excellent reusability and stability of MoS_2 in the MoS_2/Fe^{2+}/PMS system. The slight decrease in the peak intensity after the reaction was probably associated with the dissociation of Mo^{4+}.

To better understand the roles of Mo and O species in the course of MoS_2/Fe^{2+}/PMS system, XPS analysis of MoS_2 before and after reaction was performed (Fig. 5(a) and (b)). As shown in Fig. 5(a), four peaks at binding energies of 232.3 eV, 229.2 eV, 235.5 eV, and 226.5 eV correspond to the orbitals of Mo^{4+} $3d_{3/2}$, Mo^{4+} $3d_{5/2}$, Mo^{6+}, and S 2s, respectively. After the reaction, the proportion of Mo^{6+} decreased, probably due to the dissolution of MoO_3 in strong acid during the reaction or its reduction by HSO_5^- to regenerate Mo^{4+}.[40] As seen in Fig. 5(b), a peak emerged at 531.7 eV of MoS_2 before the reaction, indicating the chemisorption of the oxygen of the raw MoS_2, which has been proven to be closely related to the surface oxygen vacancies of the catalyst.[41,42] Therefore, a small amount of oxygen may have been absorbed by oxygen vacancies, and electron transfer occurred

© 2021 The Author(s). Published by the Royal Society of Chemistry

Open Access Article. Published on 08 October 2021. Downloaded on 12/29/2025 11:10:09 AM.
This article is licensed under a Creative Commons Attribution-NonCommercial 3.0 Unported Licence.

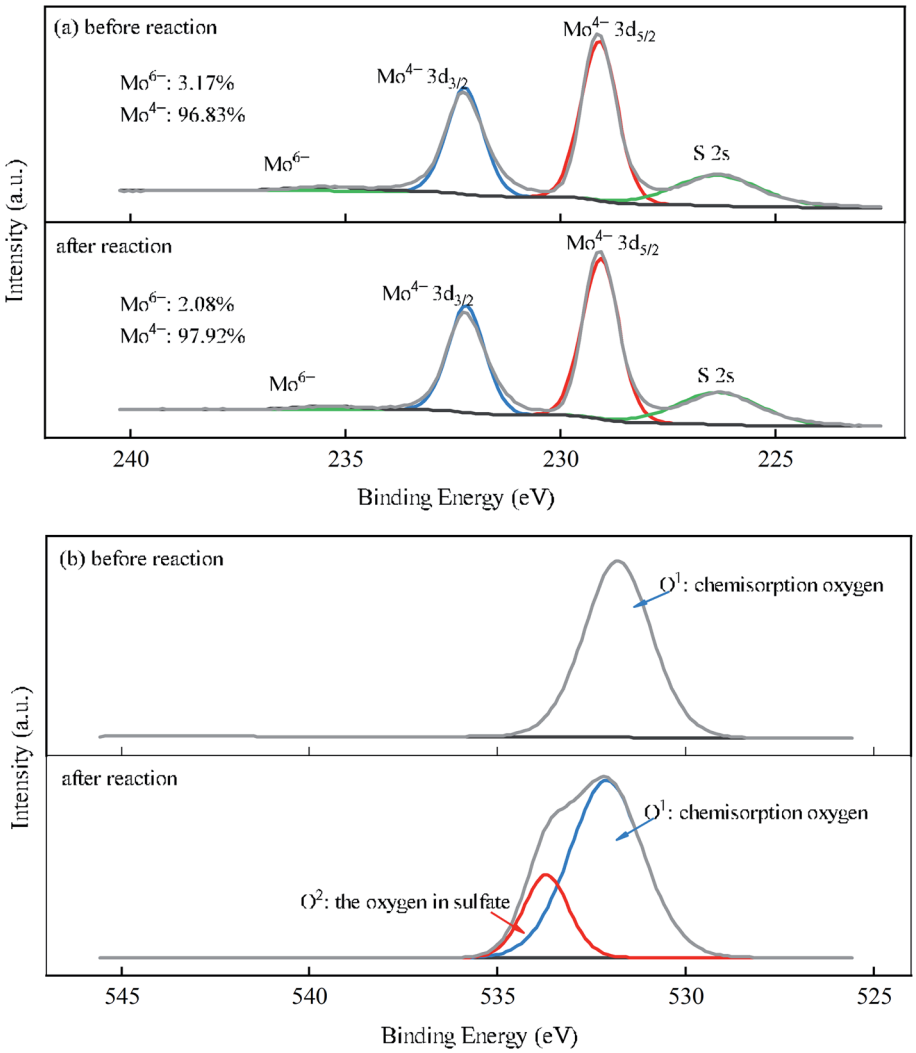

Fig. 5 XPS spectra of MoS_2 before and after the reaction for the (a) Mo 3d and (b) O 1s orbital levels.

through eqn (16).[43] After the reaction, another peak formed at 533.3 eV, which was attributed to the oxygen in sulfate (SO_4^{2-}).[42]

3.6. Proposed mechanisms of radical generation

Based on the radical species and characterization of MoS_2, the mechanisms of radical generation in the MoS_2/Fe^{2+}/PMS system can be elucidated as follows (Fig. 6). The initial activation of PMS by Fe^{2+} to generate $SO_4^{\cdot-}$ and $^{\cdot}OH$ has been widely acknowledged (eqn. (1) and (2)). The unsaturated S atoms on the surface of MoS_2 can capture protons from the solution to form H_2S and expose reductive Mo^{4+} active sites to accelerate the transformation of Fe^{3+} to Fe^{2+} (eqn (4)), which facilitates PMS activation. This was further supported by the variation of Fe^{2+} in the solution with and without MoS_2 (Fig. S3†). As seen, the concentration of Fe^{2+} sharply decreased within 2.5 min and then gradually decreased to zero at 15 min in the Fe^{2+}/PMS system. While, despite the concentration of Fe^{2+} also decreased significantly in the initial stage, and then it gradually increased along with the reaction time due to the transformation of Fe^{3+} to Fe^{2+} caused by the presence of MoS_2. Similar result was also observed by other researchers.[44–46] The reductive Mo^{4+} active sites are also directly involved in PMS activation (eqn (3)). In addition to the formation of $^{\cdot}OH$ and $SO_4^{\cdot-}$, quenching experiments and EPR analysis also confirmed the formation of $O_2^{\cdot-}$ and $^1O_2$ in the MoS_2/Fe^{2+}/PMS system. The formation of $O_2^{\cdot-}$ in the system may be attributed to PMS self-decomposition, in which electron transfer plays an important role (eqn (17) and (18)).[47] On the other hand, the edge S of MoS_2 dissociated under acidic conditions, resulting in the generation of S vacancies, which might absorb O_2 to generate $O_2^{\cdot-}$ (eqn (16)).[43] To further confirm the main formation mechanism of $O_2^{\cdot-}$ in the MoS_2/Fe^{2+}/PMS system, the degradation of PNT were carried out by sparging different gases (N_2 and O_2) (Fig. S4†). The degradation rate of PNT was only reduced by 7% when continuously sparging N_2 into the solution. While, by sparging O_2 inhibited the degradation of PNT probably due to the fast transformation of Fe^{2+} to Fe^{3+} in the presence of O_2. Therefore, PMS self-decomposition play an important role on the formation of $O_2^{\cdot-}$ in the MoS_2/Fe^{2+}/PMS system. Generally, the formation of $^1O_2$ may originate from the reaction between the generated $O_2^{\cdot-}$ and $^{\cdot}OH$ or H_2O (Eqs. (19) and (20)) as well as the self-decomposition of PMS (eqn (21)).[43,47] In addition, previous study also indicated that the formed Mo^{6+}

Open Access Article. Published on 08 October 2021. Downloaded on 12/29/2025 11:10:09 AM.
This article is licensed under a Creative Commons Attribution-NonCommercial 3.0 Unported Licence.

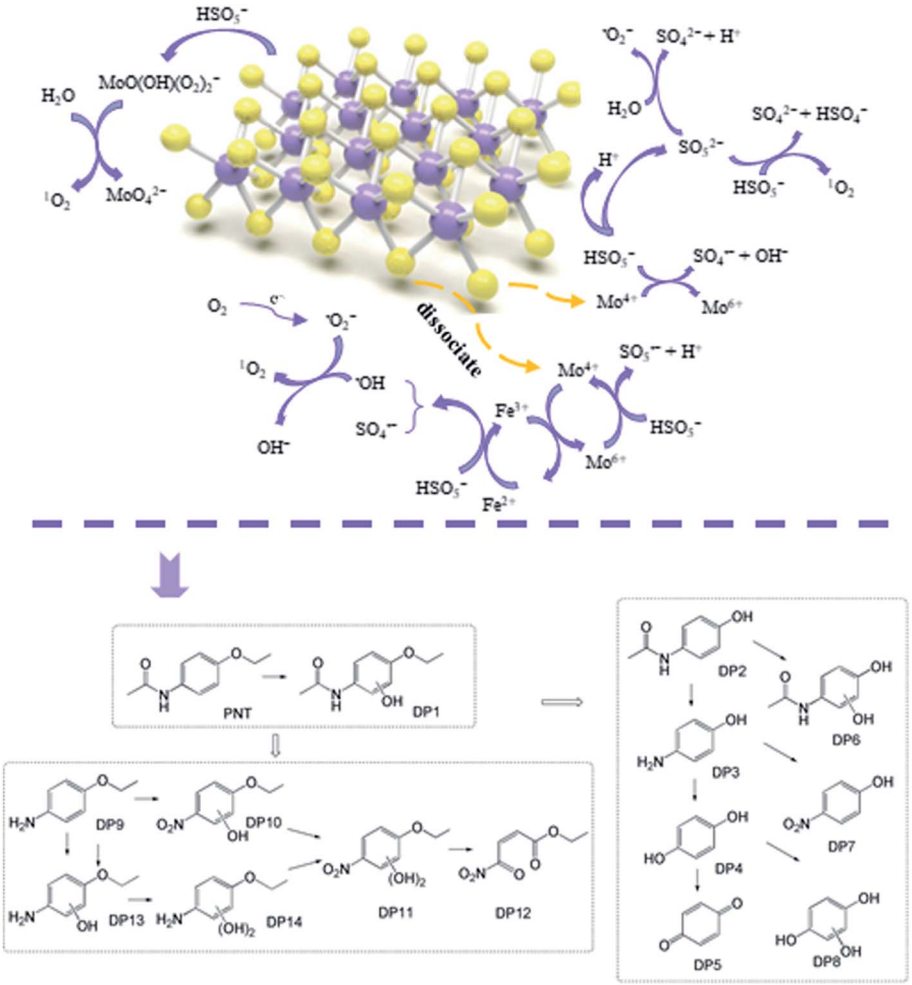

Fig. 6 Proposed reaction mechanism and transformation pathways in the MoS_2/Fe^{2+}/PMS system.

peroxo-complex may also serve as an activator of PMS to form $^1O_2$ according to eqn (22).[40]

$$O_2 + e^- \rightarrow O_2^{\bullet -} \quad (16)$$

$$HSO_5^- \rightarrow H^+ + SO_5^{2-} \quad (17)$$

$$SO_5^{2-} + H_2O \rightarrow O_2^{\bullet -} + SO_4^{2-} + H^+ \quad (18)$$

$$O_2^{\bullet -} + \cdot OH \rightarrow {}^1O_2 + OH^- \quad (19)$$

$$O_2^{\bullet -} + 2H_2O \rightarrow {}^1O_2 + H_2O_2 + 2OH^- \quad (20)$$

$$HSO_5^- + SO_5^{2-} \rightarrow HSO_4^- + SO_4^{2-} + {}^1O_2 \quad (21)$$

$$MoO(OH)(O_2)_2^- + H_2O \rightarrow MoO_4^{2-} + {}^1O_2 + H^+ \quad (22)$$

3.7. DFT calculations and transformation pathways

Fig. S5† shows the chemical structure and Fukui function index (f^0) of PNT. A higher f^0 means that the PNT sites are attacked earlier by radicals, and when the f^0 is higher, the PNT site is more vulnerable.[48] Furthermore, LC/TOF/MS was performed to identify the degradation products of PNT in the MoS_2/Fe^{2+}/PMS system. After reaction for 5 min, new peaks appeared in the total ion chromatogram (TIC) (Fig. S6†). According to the results, approximately nine degradation products were identified, and all these products are listed in Table S1.† Based on the above DFT results, the detected products and previous studies, we proposed the possible transformation pathways of PNT, as shown in Fig. 6.

The chemical structure of PNT consists of an acetyl-amino group, an ethoxy group, and an aromatic ring. The sites of 6(C) and 9(C) have high f^0 values and are easily attacked by free radicals. $SO_4^{\bullet -}$ and $^{\bullet}OH$ can react with the aromatic ring of PNT through electron transfer and hydrogen absorption to generate hydroxylated PNT. DP2, which was identified as paracetamol, a common drug and the metabolite of PNT in humans, may arise from the cleavage of the bond between 3(O) ($f^0 = 0.0639$) and 2(C) ($f^0 = 0.0138$).[49] Then, the cleavage of the C–N bond of DP2 leads to the formation of aminophenol (DP3), which could be further oxidized to hydroquinone (DP4) and benzoquinone (DP5).[50] $SO_4^{\bullet -}$ is a single-electron oxidant that readily reacts with organic matter containing electron-rich functional groups such as aromatic and aniline moieties *via* an electron transfer mechanism.[51] The amino group of DP3 is a potential reactive

© 2021 The Author(s). Published by the Royal Society of Chemistry

Open Access Article. Published on 08 October 2021. Downloaded on 12/29/2025 11:10:09 AM.
This article is licensed under a Creative Commons Attribution-NonCommercial 3.0 Unported Licence.

site for $SO_4^{\bullet-}$. Thus, the presence of nitrophenol (DP7) indicates that the amino group ($-NH_2$) in 4-aminophenol can be oxidized into a nitro group ($-NO_2$) *via* the attack of $SO_4^{\bullet-}$. This formation mechanism of nitrophenol has been previously described (Fig. S7†).[52,53] DP6 and P8 were the hydroxylated products of paracetamol and DP5, respectively. The cleavage of the bond between 11(C) ($f^0 = 0.0697$) and 10(N) ($f^0 = 0.0498$) of acetyl-amino groups leads to the formation of DP9. After the amino group of DP9 is oxidized to a nitro group, the hydroxylation reaction is initiated by the attack of $SO_4^{\bullet-}$/$^{\bullet}OH$ to form two hydroxylated products, *i.e.*, DP10 and DP11, and one open-ring product, DP12. DP13 and DP14 correspond to the mono- and dihydroxylated products of DP9, which form *via* hydroxylation driven by $^{\bullet}OH$ and/or $SO_4^{\bullet-}$ in a similar way. Therefore, the primary transformation pathways of PNT in the MoS_2/Fe^{2+}/PMS system include hydroxylation of the aromatic ring, cleavage of the C–N bond of the acetyl-amino group, and cleavage of the C–O bond of the ethoxy group.

3.8. Toxicity assessment

The TOC removal rate was only 2.8% at 15 min (Fig. S8†), indicating PNT may transform into intermediate products as discussed above rather complete mineralization. Thus, it is necessary to evaluate the toxicity of the degradation products since these products may be more toxic than their parent compound. In this study, the toxicity of PNT and its degradation products in the MoS_2/Fe^{2+}/PMS system were predicted by the ECOSAR program. According to the Globally Harmonized System of Classification and Labeling of Chemicals (GHS), the toxicity of substances can be divided into four levels, including not harmful ($LC_{50}/EC_{50}/ChV > 100$ mg L^{-1}), harmful (10 mg L^{-1} < $LC_{50}/EC_{50}/ChV \leq 100$ mg L^{-1}), toxic (1 mg L^{-1} < $LC_{50}/EC_{50}/ChV \leq 10$ mg L^{-1}) and very toxic ($LC_{50}/EC_{50}/ChV \leq 1$ mg L^{-1}), where LC_{50}, EC_{50} and ChV refer to half lethal concentration, half effective concentration and chronic toxicity, respectively.[54] As shown in Fig. 7, green algae were more sensitive to acute toxicity, whereas fish and daphnid were more sensitive to chronic toxicity. Also, chronic toxicity was more significant to three species than that of acute toxicity. As for the acute toxicity, DP6 showed 'very toxic' and PNT, DP5, DP8, DP9, DP10, DP11 and DP12 exhibited 'toxic' to green algae. As for the chronic toxicity, DP6 and DP10 were more toxic than PNT for fish. Except for DP1, DP5, DP7, DP9, DP12 and DP13, all other degradation products showed more toxic than PNT for daphnid. The characteristics of degradation products' structure exert great impact on the toxicity. Therefore, the incomplete mineralization of PNT may lead to the formation of degradation products with higher toxicity, particularly hydroxylated products or products containing amino group, which should be carefully considered in practical application.[55]

4. Conclusion

In this study, we investigated the performance and mechanism of the MoS_2-assisted Fe^{2+}/PMS process of removing phenacetin. Compared to the Fe^{2+}/PMS process, the MoS_2/Fe^{2+}/PMS process obviously enhanced PNT degradation. The best initial solution pH for the MoS_2/Fe^{2+}/PMS system for degrading PNT was 3. The optimum doses of Fe^{2+}, PMS and MoS_2 in terms of PNT degradation efficiency were determined. The presence of Cl^-, HCO_3^-, SO_4^{2-} and HA all exhibited inhibitory effects on the degradation of PNT. Quenching experiments and EPR analysis indicated that four types of reactive species, including $^{\bullet}OH$, $SO_4^{\bullet-}$, $O_2^{\bullet-}$, and $^1O_2$, were detected in the MoS_2/Fe^{2+}/PMS system. The degradation pathways were proposed by LC/TOF/MS results and supported by the calculated Fukui index, and the primary transformation pathways of PNT were proposed. This mechanism can be briefly summarized as the hydroxylation of aromatic rings, cleavage of the C–N bonds of the acetyl-amino groups, and cleavage of the C–O bonds of the ethoxy groups. Toxicity analysis showed that most of the PNT degradation

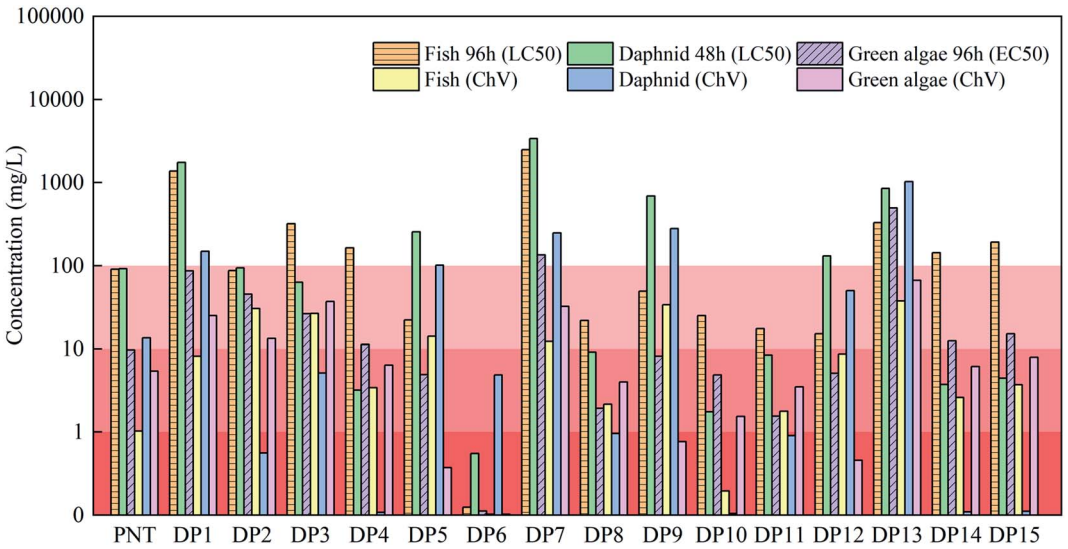

Fig. 7 Toxicity prediction of PNT and its degradation products.

Open Access Article. Published on 08 October 2021. Downloaded on 12/29/2025 11:10:09 AM. This article is licensed under a Creative Commons Attribution-NonCommercial 3.0 Unported Licence.

products are less toxic, but there are also generated products with higher toxic than that of PNT, which should be carefully considered in practical application. This study provides a deep understanding of the promoting effect of MoS_2 in the Fe^{2+}/PMS system and evaluates the characteristics and mechanism of PNT degradation in the $SO_4^{\cdot-}$-based oxidation process.

Conflicts of interest

There are no conflicts to declare.

Acknowledgements

This work was funded by the National Natural Science Foundation of China (51708348), the Scientific and Innovative Action Plan of Shanghai, China (19DZ1208204) and State Key Laboratory of Pollution Control and Resource Reuse Foundation (PCRRF18005).

References

1 C. Su, Y. Cui, D. Liu, H. Zhang and Y. Baninla, *Sci. Total Environ.*, 2020, **720**, 137652.
2 D. Wu, Q. Sui, X. Yu, W. Zhao, Q. Li, D. Fatta-Kassinos and S. Lyu, *Sci. Total Environ.*, 2021, **753**, 141653.
3 L. Bo, L. Feng, J. Fu, X. Li, P. Li and Y. Zhang, *J. Environ. Chem. Eng.*, 2015, **3**, 2203–2211.
4 Y. Gao, J. Zhou, J. Zhang, C. Li, N. Gao and D. Yin, *Sep. Purif. Technol.*, 2021, **256**, 117819.
5 C. G. Daughton and I. S. Ruhoy, *Sci. Total Environ.*, 2013, **443**, 324–337.
6 N. Taoufik, W. Boumya, M. Achak, M. Sillanpää and N. Barka, *J. Environ. Manage.*, 2021, **288**, 112404.
7 Y. Q. Gao, N. Y. Gao, D. Q. Yin, F. X. Tian and Q. F. Zheng, *Chemosphere*, 2018, **201**, 50–58.
8 J. Wang and S. Wang, *Chem. Eng. J.*, 2018, **334**, 1502–1517.
9 X. He, A. A. De La Cruz and D. D. Dionysiou, *J. Photochem. Photobiol., A*, 2013, **251**, 160–166.
10 P. Devi, U. Das and A. K. Dalai, *Sci. Total Environ.*, 2016, **571**, 643–657.
11 C. Tan, Y. Dong, L. Shi, Q. Chen, S. Yang, X. Liu, J. Ling, X. He and D. Fu, *J. Taiwan Inst. Chem. Eng.*, 2018, **83**, 74–81.
12 G. Liu, X. Li, B. Han, L. Chen, L. Zhu and L. C. Campos, *J. Hazard. Mater.*, 2017, **322**, 461–468.
13 Y. Q. Gao, J. Zhang, J. Q. Zhou, C. Li, N. Y. Gao and D. Q. Yin, *RSC Adv.*, 2020, **10**, 20991–20999.
14 A. De Luca, R. F. Dantas and S. Esplugas, *Water Res.*, 2014, **61**, 232–242.
15 S. Miralles-Cuevas, I. Oller, J. A. S. Pérez and S. Malato, *Water Res.*, 2014, **64**, 23–31.
16 A. De Luca, R. F. Dantas and S. Esplugas, *Appl. Catal., B*, 2015, **179**, 372–379.
17 W. Dong, Y. Jin, K. Zhou, S. P. Sun, Y. Li and X. D. Chen, *Sci. Total Environ.*, 2019, **688**, 513–520.
18 M. Xing, W. Xu, M. Xing, W. Xu, C. Dong, Y. Bai, J. Zeng and Y. Zhou, *Chem*, 2018, **4**, 1359–1372.
19 H. Zhou, L. Lai, Y. Wan, Y. He, G. Yao and B. Lai, *Chem. Eng. J.*, 2020, **384**, 123264.
20 B. Sheng, F. Yang, Y. Wang, Z. Wang, Q. Li, Y. Guo, X. Lou and J. Liu, *Chem. Eng. J.*, 2019, **375**, 121989.
21 D. He, Y. Cheng, Y. Zeng, H. Luo, K. Luo, J. Li, X. Pan, D. Barceló and J. C. Crittenden, *Chemosphere*, 2020, **240**, 124979.
22 S. Wang, W. Xu, J. Wu, Q. Gong and P. Xie, *Sep. Purif. Technol.*, 2020, **235**, 116170.
23 M. Du, Q. Yi, J. Ji, Q. Zhu, H. Duan, M. Xing and J. Zhang, *Chin. Chem. Lett.*, 2020, **31**, 2803–2808.
24 M. I. Kanjal, M. Muneer, A. Abdelhaleem and W. Chu, *Chin. J. Chem. Eng.*, 2020, **28**, 2658–2667.
25 A. Takdastan, B. Kakavandi, M. Azizi and M. Golshan, *Chem. Eng. J.*, 2018, **331**, 729–743.
26 Y. R. Wang and W. Chu, *J. Hazard. Mater.*, 2011, **186**, 1455–1461.
27 A. Rastogi, S. R. Al-Abed and D. D. Dionysiou, *Appl. Catal., B*, 2009, **85**, 171–179.
28 J. Yu, D. Ma, L. Mei, Q. Gao, W. Yin, X. Zhang, L. Yan, Z. Gu, X. Ma and Y. Zhao, *J. Mater. Chem. B*, 2018, **6**, 487–498.
29 H. Liu, T. A. Bruton, W. Li, J. Van Buren, C. Prasse, F. M. Doyle and D. L. Sedlak, *Environ. Sci. Technol.*, 2016, **50**, 890–898.
30 P. Neta, R. E. Huie and A. B. Ross, *J. Phys. Chem. Ref. Data*, 1988, **17**, 1027–1284.
31 C. Liang, Z. S. Wang and N. Mohanty, *Sci. Total Environ.*, 2006, **370**, 271–277.
32 M. Ahmadi and F. Ghanbari, *Mater. Res. Bull.*, 2019, **111**, 43–52.
33 X. Wu, X. Gu, S. Lu, Z. Qiu, Q. Sui, X. Zang, Z. Miao and M. Xu, *Sep. Purif. Technol.*, 2015, **147**, 186–193.
34 C. Luo, J. Jiang, J. Ma, S. Pang, Y. Liu, Y. Song, C. Guan, J. Li, Y. Jin and D. Wu, *Water Res.*, 2016, **96**, 12–21.
35 Y. Ji, Y. Fan, K. Liu, D. Kong and J. Lu, *Water Res.*, 2015, **87**, 1–9.
36 Z. Huang, P. Wu, J. Liu, S. Yang, M. Chen, Y. Li, W. Niu and Q. Ye, *Chem. Eng. J.*, 2020, **395**, 124936.
37 Q. Yi, J. Ji, B. Shen, C. Dong, J. Liu, J. Zhang and M. Xing, *Environ. Sci. Technol.*, 2019, **53**, 9725–9733.
38 H. Luo, Y. Cheng, Y. Zeng, K. Luo, D. He and X. Pan, *Sep. Purif. Technol.*, 2020, **248**, 117023.
39 H. Sun, F. He and W. Choi, *Environ. Sci. Technol.*, 2020, **54**, 6427–6437.
40 Y. Zhang, J. Niu and J. Xu, *Chem. Eng. J.*, 2020, **381**, 122718.
41 M. C. Biesinger, L. W. M. Lau, A. R. Gerson and R. S. C. Smart, *Appl. Surf. Sci.*, 2010, **257**, 887–898.
42 J. Li, J. Fang, L. Gao, J. Zhang, X. Ruan, A. Xu and X. Li, *Appl. Surf. Sci.*, 2017, **402**, 352–359.
43 S. Sun, Y. Gu, Y. Wang and Y. Liu, *Chem. Phys. Lett.*, 2020, **752**, 137557.
44 S. Qu, W. Wang, X. Pan and C. Li, *J. Hazard. Mater.*, 2020, **384**, 121494.
45 Y. Li, D. D. Cheng, Y. Luo and L. X. Yang, *Rare Met.*, 2021, **40**, 3543–3553.
46 X. X. Ji, H. F. Wang and P. J. Hu, *Rare Met.*, 2019, **38**, 783–792.

© 2021 The Author(s). Published by the Royal Society of Chemistry

Open Access Article. Published on 08 October 2021. Downloaded on 12/29/2025 11:10:09 AM.
This article is licensed under a Creative Commons Attribution-NonCommercial 3.0 Unported Licence.

47 B. Liu, W. Song, H. Wu, Y. Xu, Y. Sun, Y. Yu and H. Zheng, *Chem. Eng. J.*, 2020, **400**, 125947.
48 X. Zhao, P. Du, Z. Cai, T. Wang, J. Fu and W. Liu, *Environ. Pollut.*, 2018, **232**, 580–590.
49 M. Xiao and Y. Zhang, *Chemosphere*, 2016, **152**, 17–22.
50 M. Noorisepehr, B. Kakavandi, A. A. Isari, F. Ghanbari, E. Dehghanifard, N. Ghomi and F. Kamrani, *Sep. Purif. Technol.*, 2020, **250**, 116950.
51 L. Zhou, X. Yang, Y. Ji and J. Wei, *Sci. Total Environ.*, 2019, **692**, 201–208.
52 M. Mahdi Ahmed, S. Barbati, P. Doumenq and S. Chiron, *Chem. Eng. J.*, 2012, **197**, 440–447.
53 Y. Yang, X. Lu, J. Jiang, J. Ma, G. Liu, Y. Cao, W. Liu, J. Li, S. Pang, X. Kong and C. Luo, *Water Res.*, 2017, **118**, 196–207.
54 M. Xu, J. Deng, A. Cai, C. Ye, X. Ma, Q. Li, S. Zhou and X. Li, *Chem. Eng. J.*, 2021, **413**, 127533.
55 X. Zheng, Y. Li, J. Yang and S. Cui, *Chem. Eng. J.*, 2021, **422**, 130105.

© 2021 The Author(s). Published by the Royal Society of Chemistry